Matilainen, Noora; Kataja, Juhani; Laakso, Ilkka

Predicting the hotspot location and motor threshold prior to transcranial magnetic stimulation using electric field modelling

Published in:
Physics in Medicine and Biology

DOI:
10.1088/1361-6560/ad0219

Published: 07/01/2024

Document Version
Publisher's PDF, also known as Version of record

PAPER • OPEN ACCESS

Predicting the hotspot location and motor threshold prior to transcranial magnetic stimulation using electric field modelling

To cite this article: Noora Matilainen *et al* 2024 *Phys. Med. Biol.* **69** 015012

IOP Publishing Phys. Med. Biol. 69 (2024) 015012 https://doi.org/10.1088/1361-6560/ad0219

Physics in Medicine & Biology

IPEM Institute of Physics and Engineering in Medicine

OPEN ACCESS

RECEIVED
26 May 2023

REVISED
3 October 2023

ACCEPTED FOR PUBLICATION
10 October 2023

PUBLISHED
22 December 2023

PAPER

Predicting the hotspot location and motor threshold prior to transcranial magnetic stimulation using electric field modelling

Noora Matilainen[1], **Juhani Kataja**[1] and **Ilkka Laakso**[1,2]

[1] Department of Electrical Engineering and Automation, Aalto University, Espoo, Finland
[2] Aalto Neuroimaging, Aalto University, Espoo, Finland

E-mail: noora.matilainen@aalto.fi

Keywords: TMS, dosimetric modelling, hotspot, transcranial magnetic stimulation, electric field, motor threshold, motor evoked potential

Abstract

Objective. To investigate whether the motor threshold (MT) and the location of the motor hotspot in transcranial magnetic stimulation (TMS) can be predicted with computational models of the induced electric field. *Approach.* Individualized computational models were constructed from structural magnetic resonance images of ten healthy participants, and the induced electric fields were determined with the finite element method. The models were used to optimize the location and direction of the TMS coil on the scalp to produce the largest electric field at a predetermined cortical target location. The models were also used to predict how the MT changes as the magnetic coil is moved to various locations over the scalp. To validate the model predictions, the motor evoked potentials were measured from the first dorsal interosseous (FDI) muscle with TMS in the ten participants. Both computational and experimental methods were preregistered prior to the experiments. *Main results.* Computationally optimized hotspot locations were nearly as accurate as those obtained using manual hotspot search procedures. The mean Euclidean distance between the predicted and the measured hotspot locations was approximately 1.3 cm with a 0.8 cm bias towards the anterior direction. Exploratory analyses showed that the bias could be removed by changing the cortical target location that was used for the prediction. The results also indicated a statistically significant relationship ($p < 0.001$) between the calculated electric field and the MT measured at several locations on the scalp. *Significance.* The results show that the individual TMS hotspot can be located using computational analysis without stimulating the subject or patient even once. Adapting computational modelling would save time and effort in research and clinical use of TMS.

1. Introduction

Transcranial magnetic stimulation (TMS) is a non-invasive brain stimulation method for researching the brain functionality and for clinical use, where TMS is used to treat brain disorders such as depression (Baeken *et al* 2019) and chronic pain (Stilling *et al* 2019). In TMS, a pulse of electric current in a coil located above the scalp generates a magnetic field, which in turn induces an electric field in the brain. This induced electric field can excite or inhibit the targeted brain area (Hallett 2000, Siebner *et al* 2022).

The exact cortical location(s) activated by TMS depend on the strength and direction of the induced electric field. Unfortunately, the induced electric fields cannot be directly measured. Therefore, they are usually simulated using a computational dosimetric models constructed from structural magnetic resonance image (MRI) data (Gomez-Tames *et al* 2020). Modern dosimetric models factor in several different aspects, such as coil location and direction, individual cortical structure, conductivity of biological tissues and body fluids, and realistic neurone models (Thielscher *et al* 2011, Aberra *et al* 2020). Precise estimation of the induced electric field is, however, fairly challenging because of various intricacies in the brain structure that affect the electric field and differ between individuals (Gomez-Tames *et al* 2020).

In general clinical TMS procedures and in research studies, the TMS parameters are typically adjusted individually based on the motor threshold (MT) and optimal coil location (hotspot), which need to be measured at the start of the protocol (Rossini *et al* 2015). However, this can be time-consuming as several magnetic pulses are required to measure the MT and to ensure that the TMS coil will be optimally positioned for stimulating the cortical target location. Additionally, this procedure is susceptible to variations, which affect the outcome and repeatability, such as the operator's subjective decision making (Sollmann *et al* 2013). Therefore, there have been attempts to streamline the process, for example, with an automated hotspot detection procedure (Meincke *et al* 2016, Tervo *et al* 2020). Although these methods eliminate the user-specific variation, they still require multiple stimulations. Dosimetric models could potentially improve the clinical practice by providing information before stimulation. With dosimetric models, the stimulation intensity and location could be predetermined making the initial MT and hotspot search redundant, which would shorten the time required for the TMS procedure.

Previous studies have used dosimetric models to develop methods for estimating the locations that TMS activates in the brain (Bungert *et al* 2017, Aonuma *et al* 2018, Laakso *et al* 2018, Weise *et al* 2020, Kataja *et al* 2021). These methods could potentially be used inversely to predetermine important factors such as hotspot location and MT prior to TMS. However, these methods have not yet been used prospectively, and have only been used to analyse existing measurement data.

This preregistered study (https://doi.org/10.17605/OSF.IO/MA2JT) aims to improve the TMS procedure by providing a method that predicts the hotspot coil location and direction prior to the TMS. Additionally, we investigate whether the MT can be estimated from dosimetric models. We test two hypotheses: H1) Hotspot coil location for the the first dorsal interosseous (FDI) muscle can be predicted with 1 cm accuracy prior to the TMS by computationally optimizing the coil location and direction to produce the largest normal component to the grey matter surface of the electric field at the FDI cortical location ($E_{n,\mathrm{FDI}}$), and H2) Active motor threshold (AMT) values are inversely proportional to $E_{n,\mathrm{FDI}}$.

These hypotheses were selected based on a previous study (Laakso *et al* 2018) that estimated the location of the cortical activation site of the FDI muscle using TMS measurement and retrospective dosimetric analysis. The study also demonstrated a strong inverse relationship between the electric field normal component at the estimated activation site ($E_{n,\mathrm{FDI}}$) and the measured resting and active MTs. This indicated that it would be possible to use dosimetric models to predetermine the location and direction of the magnetic coil so that $E_{n,\mathrm{FDI}}$ is maximized. The location with the maximal $E_{n,\mathrm{FDI}}$ should correspond to the actual measured hotspot, and moving the coil away from the predetermined optimal location should increase the MT proportionally to the inverse of $E_{n,\mathrm{FDI}}$. Both hypotheses can be tested by first performing the computational analysis, and then confirming the model predictions in experiments.

2. Materials and methods

2.1. Participants

The data were collected from 10 healthy right-handed participants (5 female, 5 male, mean age $\pm$ SD $= 30.0 \pm 4.2$, age range: 26–40) in accordance with the sampling plan in the preregistration. All participants gave their written consent for participation. One participant was excluded from the first analysis as no motor evoked potentials (MEPs) were visible with 50% stimulator output, which was the predetermined intensity used in the measurements. Another participant did not participate in the second study. Therefore, both studies had nine participants for the analysis. The study was approved by the Aalto University Research Ethics Committee (decisions D/574/03.04/2022 and D/1006/03.04/2022). All procedures were conducted in accordance with the Declaration of Helsinki.

2.2. Magnetic resonance imaging

T1- and T2-weighted MR images were acquired using a 3 T MRI scanner (Magnetom Skyra; Siemens, Ltd, Erlangen, Germany) with following parameters. T1: TR/TE/TI/FA/FOV/voxel size/slice number = 1800 ms/1.99 ms/800 ms/9°/256 mm/1 × 1 × 1 mm/176; and T2: TR/TE/FOV/voxel size/slice number = 3200 ms/412 ms/256 mm/1 × 1 × 1 mm/176. The data were measured at AMI Centre, Aalto NeuroImaging, Aalto University School of Science.

2.3. Cortical reconstruction and volume conductor models

The MR images were segmented into different tissue types using a semi-automatic pipeline described in Laakso *et al* (2015). In the pipeline, non-brain tissues were segmented from T1- and T2-weighted images, and the pial (grey matter) surface and the grey–white matter boundary were reconstructed from T1-weighted images using the FreeSurfer image analysis software (Dale *et al* 1999, Fischl *et al* 1999). FreeSurfer was also used to generate a

nonlinear surface-based mapping between the individual brain surface and the surfaces of an average brain template. In this study, the average brain was the Montreal neurological institute (MNI) ICBM 2009a nonlinear asymmetric template (Fonov *et al* 2009, 2011).

Volume conductor models were generated from these segmented images by voxelizing them into cubical elements with a spatial resolution of 0.5 mm. Electric conductivity values were assigned to the voxels similarly to Laakso *et al* (2018) (unit: S/m): grey matter (0.215), white matter (0.142), cerebrospinal fluid (1.79), compact and spongy bone (0.009 and 0.034), subcutaneous fat (0.15), scalp (0.43), muscle (0.18), dura mater (0.18), and blood (0.7). Sensitivity analysis of the conductivity values was not necessary in our case, as TMS electric fields are not strongly affected by uncertainty in conductivity values (Saturnino *et al* 2019).

2.4. Calculation of the induced electric field

The induced electric fields were estimated computationally with the finite-element method (FEM) for each participant. The procedure for the calculations is described in Laakso *et al* (2018). In brief, a model of the figure-eight coil was placed on the preferred location on the head surface over the left hemisphere. From there, the induced electric field was determined using the FEM with a uniform grid of first-order cubical elements with a 0.5 mm edge length and the individual volume conductor model. The field was calculated everywhere in the head and then interpolated to a surface at a depth of 2 mm below the pial surface for analysis and visualization in order to avoid the staircase approximation error at the tissue boundary between grey matter and cerebrospinal fluid.

2.5. Optimization of the coil location and direction

The cortical target location was preregistered to be $[-41, -7, 63]$ in the MNI coordinates. This location is a group-average activation site of the FDI muscle from Laakso *et al* (2018). For each individual participant, the cortical target location corresponding to the MNI coordinates was obtained with FreeSurfer.

For each participant, the optimal coil location and direction were predetermined as the combination of a point on the scalp and direction that induce the largest electric field normal component at the preregistered cortical target location (figure 1). To speed up the calculations, the procedure for finding the optimal coil location and direction consisted of two parts: calculations with a coarse and fine grid. The coarse grid first provided a rough estimate of the location, after which the fine grid was used for more accurate estimation.

First, the electric field normal components at the preregistered cortical target location were calculated for modelled coil locations in a 11×11 grid with 1 cm distance between adjacent points. For this coarse grid, a 2 mm edge length was used for the voxel size for FEM calculations. The centre point of the grid was the closest point to the preregistered cortical target location on the scalp. The grid was adjusted to the scalp surface. The coil was placed tangentially to the scalp, and the direction at each modelled coil location was optimized to maximize the electric field normal component. Starting from the posterior-anterior direction, the coil was rotated iteratively until the electric field normal component at the cortical target point was maximal.

Then, the point on the scalp that produced the highest electric field normal component at the preregistered cortical target location was selected as the centre point for the next set of calculations following the same approach but with a 11×11 grid with 2 mm distance between adjacent points. From this, the point with the highest electric field normal component at the preregistered cortical target location was selected as the predicted optimal coil location and the direction as the predicted optimal direction in that point.

The predicted optimal coil location and direction were added to the MR images as a marker prior to the experiment to aid the positioning of the coil during neuronavigation.

2.6. TMS and EMG recordings

TMS was performed with a monophasic Magstim 200^2 stimulator (Magstim Company, UK). The TMS coil was eight-shaped with two adjacent round wings of 9 cm diameter. The coil location and orientation were tracked and recorded with the Visor2 TMS neuronavigation system (ANT Neuro, Enschede, the Netherlands). The data were measured at Aalto TMS, Aalto NeuroImaging, Aalto University School of Science.

MEPs were recorded with NeurOne EMG system (NeurOne, MEGA Electronics Ltd, Finland) and disposable Ag/AgCl surface electrodes. The electrodes were placed on the right hand FDI muscle. The recorded electromyography (EMG) signals were sampled at 5 kHz and high-pass filtered with 10 Hz cutoff frequency.

2.7. Experimental setup

Our TMS measurements consisted of two parts: the first was to validate the predicted optimal coil location and the second was to analyse the relationship between the AMT and the $E_{n,\mathrm{FDI}}$ (figure 2). In both parts, the participant was sitting on a chair with their hands positioned comfortably on a pillow placed on their lap. Their head was supported by a neck rest. The neuronavigated TMS was delivered over their left cerebral hemisphere.

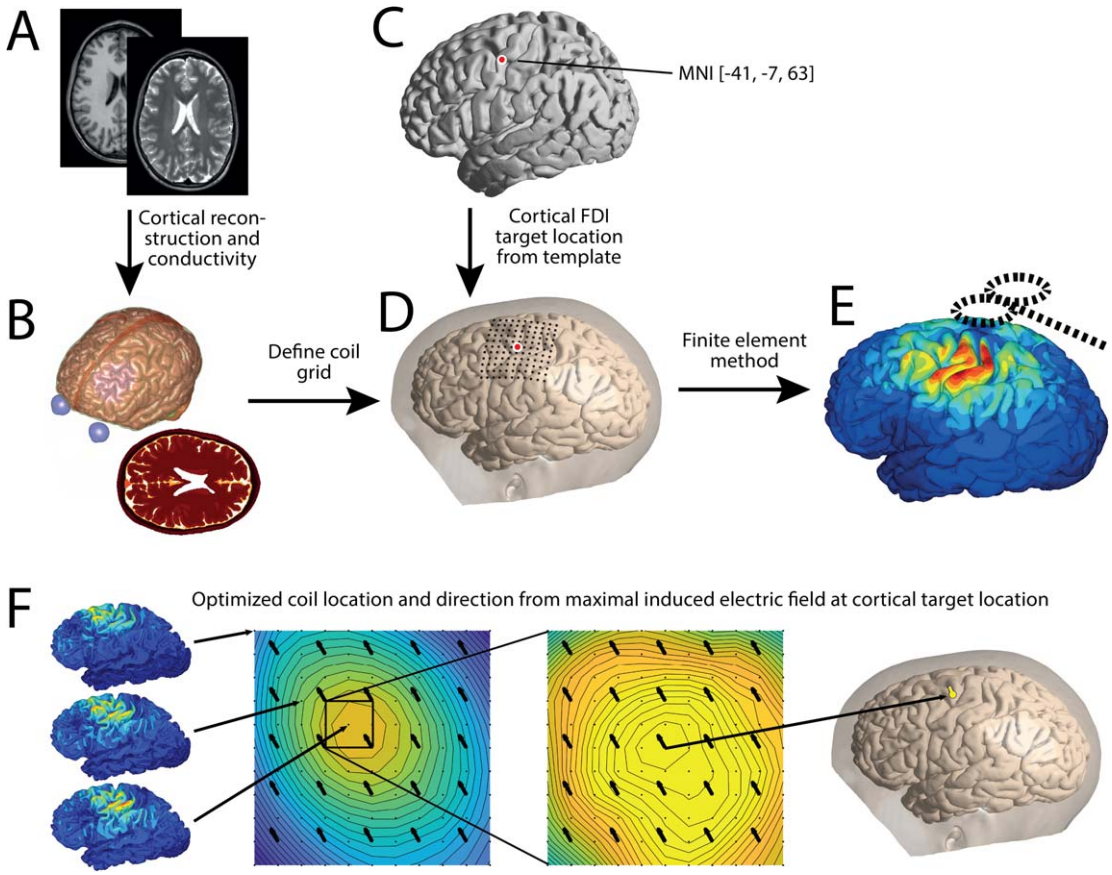

Figure 1. Prediction of the hotspot coil location and direction. (A) T1- and T2-weighted MR images were used to create (B) an individual cortical reconstruction with conductivity. (C) The preregistered cortical target location of the FDI muscle from the template brain was mapped to the (D) individual brain, and an 11 × 11 grid of 1 cm resolution was placed on top of it so that its centre point coincided scalp location closest to the mapped FDI point. (E) Individualized induced electric fields were computed using dosimetric models at each grid point. (F) The normal component of the electric field was calculated at the cortical FDI target location for each grid point, and then the calculations were repeated with a finer grid with the point that induced the strongest normal component as the centre and 2 mm grid resolution. The strongest point from this was selected as the predicted optimal coil location.

The participant's head together with the coil was 3D scanned (Artec Leo, Artec 3D, Luxembourg) to validate the coil location measured by the navigation system. If necessary, the recorded coil locations were corrected using 3D scan data for further computational analysis.

In the first part of the study, three TMS pulses were delivered in the predetermined optimal coil location and 20 locations within a 2 cm radius around it with approximately 5 s inter-stimulus interval (ISI). The stimulus intensity was 50% of the maximum stimulator output (MSO). The mean MEP amplitude was calculated in each location. The MEP amplitude was defined as the peak-to-peak distance between the negative and positive peak in the EMG waveform. The measured hotspot was defined as the location that produced the largest mean MEP amplitude. The optimized coil direction was validated by testing it against two other directions that were approximately 20 degrees counterclockwise and clockwise from the optimized direction.

In the second part of the study, the left cerebral hemisphere was stimulated in nine locations with TMS in a 3 × 3 grid (4 cm × 4 cm). The central location was the predetermined optimal coil location. These predetermined coil locations were marked on the MR images for neuronavigation during TMS. The coil direction was selected by measuring thresholds from three different directions. First, the threshold was recorded from the predicted direction, and second, from a direction approximately 30 degrees counterclockwise from the prediction. The third direction was either clockwise from the first or counterclockwise from the second, based on whichever of the first two produced the lower threshold. Finally, the direction that produced the lowest threshold was selected and used for the eight other locations. The coil was positioned using a mechanical holder. During stimulation, the participant's task was to contract their FDI muscle by applying a constant pressure on a 10 cm diameter cork ball with their fingers. Participants were instructed to observe their EMG activation from the screen in front of them and keep the peak-to-peak amplitude at 200 μV.

AMT was determined for each location by delivering 10 pulses per intensity with 2 s ISI. The intensity was started from 16% of the MSO and increased by three percentage points until either the activation was evident or a preselected limit of 61% of the MSO was reached. AMT intensities were defined as the minimum intensity

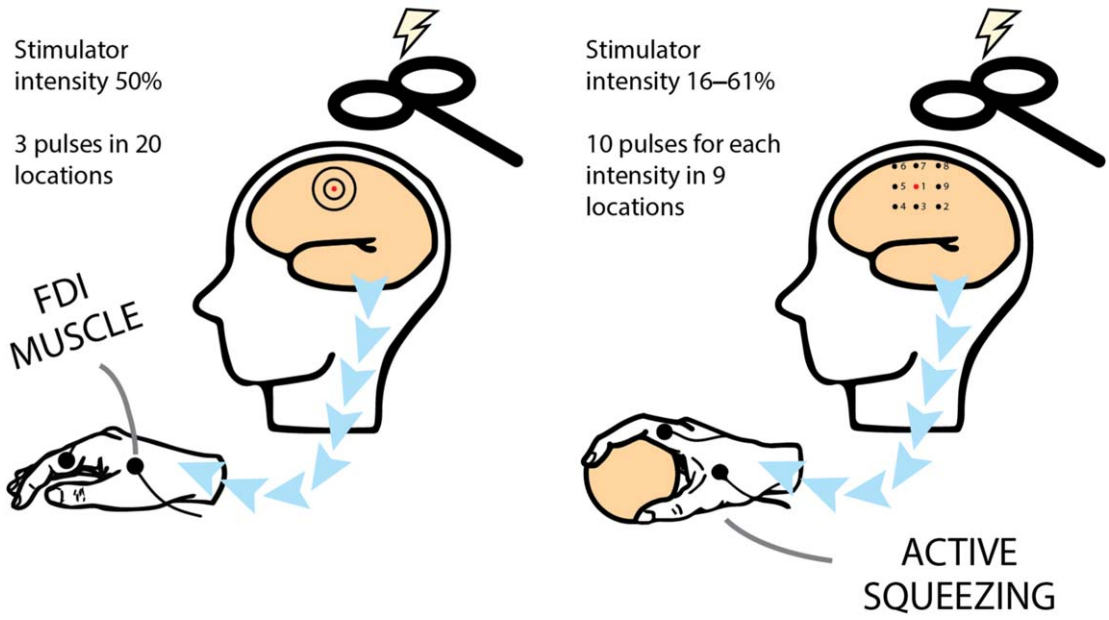

Figure 2. Experimental setup with two measurements. The first measurement was to validate the predicted optimal coil location for the FDI muscle. In that, 3 TMS pulses were delivered in the predicted optimal coil location and 20 locations in a 2 cm radius around it with 50% stimulator output intensity. The second measurement was to investigate the relationship between the AMT and the inverse of the electric field at the cortical FDI target location. In that, 9 locations in 3 × 3 grid (4 cm×4 cm) with the predicted optimal coil location as the centre were stimulated with active muscle contraction. Stimulator intensity was increased from 16% with the increase of 3 percentage points until the MEP was evident or the predetermined upper limit of 61% was reached. 10 pulses were delivered with every intensity.

required to elicit TMS MEPs with amplitude of at least 200 μV in at least 50% of trials in the FDI muscle. Active muscles were used to lower the required MT and to stabilise the modulatory effect of the ISI on the MEP amplitude (Matilainen *et al* 2022).

2.8. Data processing and statistical analysis

For the analysis, as stated in the preregistration, we used the recorded coil locations, that may slightly differ from the pre-computed locations, to calculate the $E_{n,\mathrm{FDI}}$ values. All statistical tests were performed in MATLAB 2022b (Mathworks inc.).

2.8.1. Preregistered hypotheses

For the first hypothesis, the differences in lateral-medial and posterior-anterior directions were calculated between the measured hotspot and the predicted optimal coil location. The mean and SD were calculated for the differences. We used Student's two-tailed t-tests to investigate if the means are zero to detect bias. Chi-squared test for standard deviation (one sided) was used to investigate whether the standard deviations are smaller than 1 cm. Preregistered power calculations based on the data from Laakso *et al* (2018) indicated that the test had a statistical power of 0.79 for nine subjects.

For the second hypothesis, a linear mixed effect model was used to analyse the relationship between the AMT and the inverse $E_{n,\mathrm{FDI}}$ (inv$E_{n,\mathrm{FDI}}$). This model allows non-independent observations and considers inter-subject variability. Model's specification was 'AMT $\sim$ inv$E_{n,\mathrm{FDI}}$ + (1+inv$E_{n,\mathrm{FDI}}$ | Subject)'. Maximum likelihood was used as the estimation method to fit model coefficients. As stated in the preregistration, random correlations were dropped from the model to enable it to converge properly. Statistical significance of the fixed effects were tested with likelihood ratio test against the model without inv$E_{n,\mathrm{FDI}}$. Potential outliers were detected using the generalized extreme Studentized deviate test for the model residuals, and if any were found, they were left out of the model fit.

2.8.2. Exploratory analyses

The results of the preregistered analyses suggested that the preregistered cortical target location was possibly inaccurate. To study the effect of the cortical target location, we derived new exploratory cortical target locations

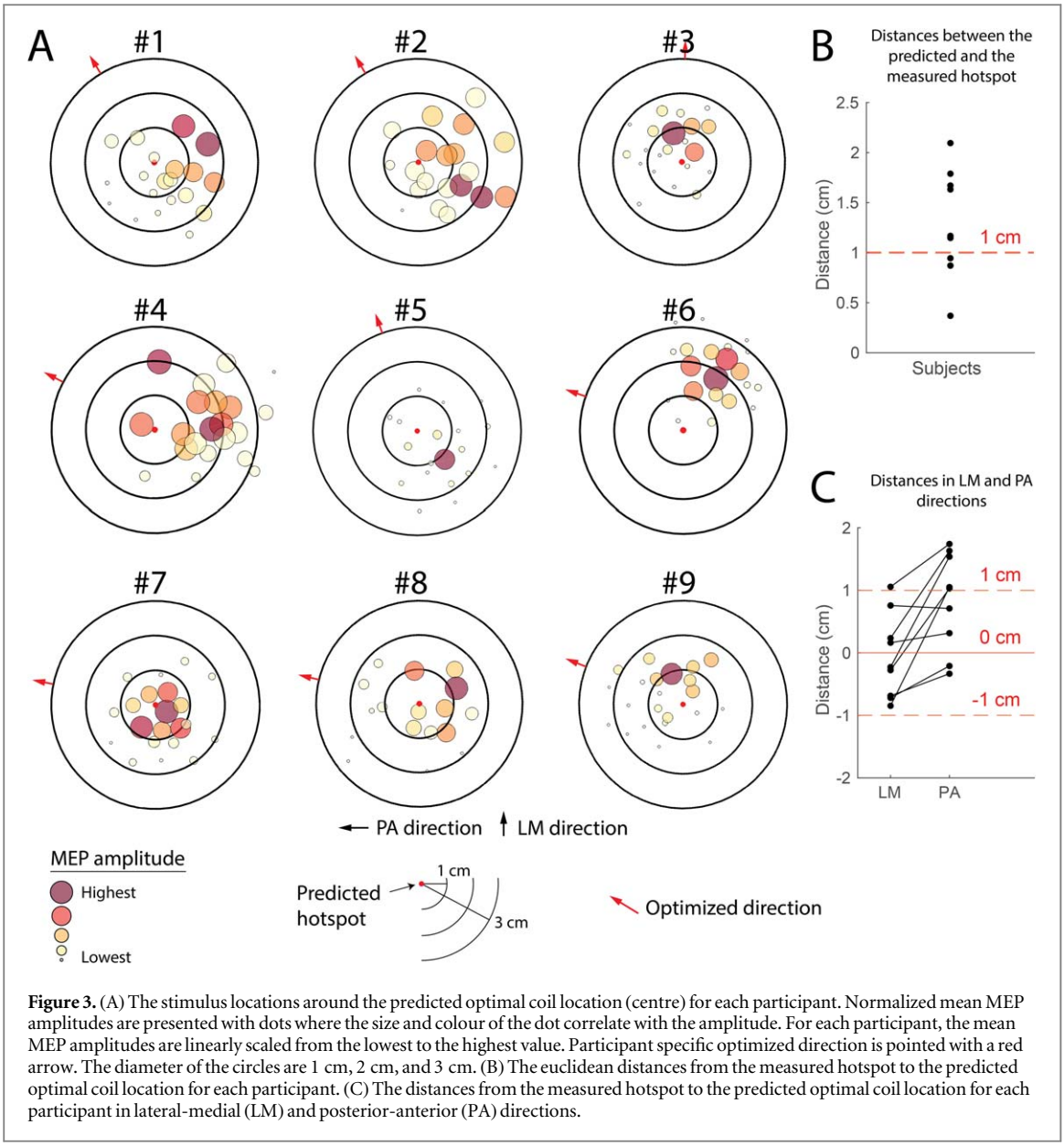

Figure 3. (A) The stimulus locations around the predicted optimal coil location (centre) for each participant. Normalized mean MEP amplitudes are presented with dots where the size and colour of the dot correlate with the amplitude. For each participant, the mean MEP amplitudes are linearly scaled from the lowest to the highest value. Participant specific optimized direction is pointed with a red arrow. The diameter of the circles are 1 cm, 2 cm, and 3 cm. (B) The euclidean distances from the measured hotspot to the predicted optimal coil location for each participant. (C) The distances from the measured hotspot to the predicted optimal coil location for each participant in lateral-medial (LM) and posterior-anterior (PA) directions.

similarly to the study of Laakso *et al* (2018) and repeated the analysis above for these new target locations. The more detailed description of the analyses is written in the results section.

3. Results

The results of the preregistered analyses are reported first, followed by the results of exploratory analyses.

3.1. Confirmatory: measured and predicted optimal coil location and direction

The predicted optimal coil locations were 0.37–2.1 cm (mean 1.3 cm, SD 0.54 cm) away from the measured hotspot locations. Figure 3 shows the locations and normalized MEP amplitudes of the stimulations relative to the predicted coil location.

The distances between the predicted optimal coil location and the measured hotspot location in lateral-medial (LM) and posterior-anterior (PA) directions were −0.85 to 1.1 cm (mean 0.06 cm, SD 0.67 cm) and −0.33 to 1.7 cm (mean 0.83 cm, SD 0.77 cm), respectively (figure 3). Student's two-tailed t-tests showed significant bias between the predicted and measured locations in the PA direction ($t(8) = 3.2$, $p = 0.01$) but not in the LM direction ($t(8) = 0.27$, $p = 0.79$). These results suggested that the predicted optimal coil location was biased to the anterior direction compared to the measured hotspot location.

Table 1. Active motor threshold (AMT) values as percentage of maximum stimulator output for each subject and coil location. Coil locations are numbered as in figure 2. Missing values indicate cases where the AMT is greater than 61%. They are treated as 61% in the calculation of the mean, median, and standard deviation (SD). Bolding shows the smallest thresholds for each subject. A Wilcoxon signed-rank test indicates that the median thresholds were statistically significantly smaller (**: $p < 0.01$, *: $p < 0.05$) than those of the predicted optimal coil location (OPT).

	Location								
	1 (OPT)	2	3	4	5	6	7	8	9
Subject 1	**31**	**31**	37	58	40	40	34	**31**	34
Subject 2	**25**	28	37	49	28	34	28	34	31
Subject 3	37	40	49	—	46	52	37	40	**34**
Subject 4	28	43	40	—	**25**	31	28	58	31
Subject 5	**28**	46	31	43	34	34	37	52	43
Subject 6	**31**	**31**	34	37	37	55	52	61	**31**
Subject 7	34	46	37	37	**28**	37	37	46	37
Subject 9	**28**	34	49	43	46	37	34	37	31
Subject 10	**34**	55	43	—	52	—	43	58	55
Mean	31	39	40	50	37	42	37	46	36
Median	31	40**	37**	49**	37*	37**	37**	46**	34*
SD	4	9	6	10	9	11	7	11	8

While the sample SDs of the distances between the measured hotspot and the predicted coil location were smaller than 1 cm, Chi-square test did not support the SDs being statistically significantly smaller than 1 cm (LM: $\chi^2(8, N = 9) = 3.6, p = 0.11$, PA: $\chi^2(8, N = 9) = 4.8, p = 0.22$).

For eight subjects, the optimized direction produced the largest mean MEP amplitude compared to directions 20 degrees clockwise and counterclockwise from the optimized direction (figure 3(A)). For subject 3, a direction 20 degrees counterclockwise from the optimized direction produced a larger mean MEP amplitude than the optimized direction.

3.2. Confirmatory: the relationship between E_nFDI and AMT

The measured AMTs for each subject and coil location are reported in table 1. The first location corresponds to the predicted optimal coil location, and the others populate the 3 × 3 grid counterclockwise starting from the bottom-left corner (figure 2). The AMT could not be measured in four cases, because it exceeded the preselected limit of 61% of the MSO. On average, the first coil location, corresponding to the predicted optimal coil location, produced the smallest AMT (Wilcoxon signed-rank tests, all $p < 0.05$). The differences between the recorded coil and the pre-computed coil locations were 2.1–18.9 mm (mean 6.6 mm, median 3.3 mm, SD 5.7 mm).

The $E_{n,\mathrm{FDI}}$ values were calculated for each subject and coil location corresponding to the measured 78 AMT values (table 1). The data were then input into a linear mixed effect model to investigate the relationship between the AMT and $E_{n,\mathrm{FDI}}$. Four outliers were left out from the model fit. The fitted model was of the form:

$$y_{ij} = \alpha + A_j + \frac{\beta + B_j}{E_{ij}} + \epsilon_{ij}, \tag{1}$$

where i is the coil location, j is the participant, y_{ij} is the AMT in terms of the MSO, E_{ij} is $E_{n,\mathrm{FDI}}$ calculated at the MSO, and α and β are the fixed effect coefficients. The participant-specific coefficients A_j and B_j and error term ϵ_{ij} follow normal distributions with zero mean and standard deviations of σ_a, σ_b, and σ_ϵ, respectively:

$$A_j \sim N(0, \sigma_a), \qquad B_j \sim N(0, \sigma_b), \qquad \epsilon_{ij} \sim N(0, \sigma_\epsilon). \tag{2}$$

The estimates for these parameters are listed in table 2. Figure 4(A) illustrates the relationship between the AMT and $E_{n,\mathrm{FDI}}$ obtained from the model. A likelihood ratio test indicated that $E_{n,\mathrm{FDI}}$ had a statistically significant effect on the AMT ($\chi^2(1) = 12.34, p < 0.001$).

Despite the statistically significant effect of $E_{n,\mathrm{FDI}}$, the present model provided only limited support for the hypothesis (H2) that the AMT was inversely proportional to $E_{n,\mathrm{FDI}}$. This could be observed by examining the model coefficients reported in table 2. Firstly, intercept α differed significantly from zero, which was evident from its confidence interval. Secondly, the effect of the electric field term, characterized by coefficient β, was relatively small compared to the intercept ($E_{n,\mathrm{FDI}}$ varied between 50 and 250 V m^{-1}). Taken together, the model indicated that the AMT was always approximately 30% of the MSO added with a small electric-field dependent correction. For example, a change of $E_{n,\mathrm{FDI}}$ from 200 to 100 V m^{-1} would lead to an approximate change in the AMT from 35% to 41% of the MSO, depending on the subject. This was markedly different from the ideal

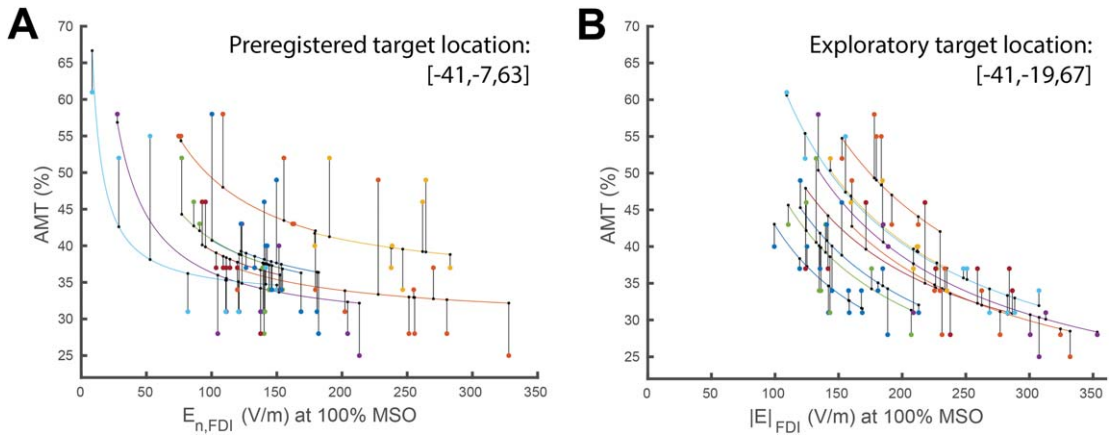

Figure 4. (A) The relationship between the AMT and the $E_{n,\mathrm{FDI}}$ at the preregistered cortical FDI target location. (B) The relationship between the AMT and the $|E|_{\mathrm{FDI}}$ at the exploratory cortical FDI target location.

Table 2. Coefficient estimates for the linear mixed effect model fit. The model was fitted for two cortical target locations, A and B, which correspond to the preregistered target location and that obtained from exploratory analyses. %MSO = percentage of maximum stimulator output. CI = confidence interval.

		A. Preregistered target		B. Exploratory target	
Parameter	Unit	Estimate	95% CI	Estimate	95% CI
α	%MSO	31	27–35	16	11–21
β	V/m	10.35	4.99–15.72	42.51	31.86–53.16
σ_a	%MSO	3	1–9	2	0–26
σ_b	V/m	4.77	2.11–10.75	9.82	5.52–17.49
σ_ϵ	%MSO	7	5–8	5	4–6

scenario (hypothesis H2), where the AMT should double when the coil is moved so that the electric field is halved.

In contrast, during the development of the preregistered hypotheses of this paper, we used the AMT and electric field data obtained from a previous study (Laakso *et al* 2018) to select the linear mixed effects model. During development, the model indicated that the intercept was not different from zero ($\alpha = 0.02$ [95% CI: $-0.02, 0.07$]) and $\beta = 67.7$ V m^{-1} [95% CI: 53.5, 81.9], indicating a near-ideal relationship between $E_{n,\mathrm{FDI}}$ and the AMT.

We hypothesized that the poorer than expected fit between the electric field and the AMT was due to a mismatch in the cortical target location that was used to calculate the electric field values for the analysis. The same reason could possibly explain why the predicted optimal coil location was more anterior compared to the measured hotspot location.

3.3. Exploratory: improved estimate of the cortical target location using correlation analysis

Next, we explored which target location in the cortex would produce a better agreement between the electric field and AMT and whether the new target location would produce an improved prediction of the optimal coil location.

For the analysis, we used the method of Laakso *et al* (2018). In the method, the electric field data (normal component or magnitude) of each subject is first mapped to the surface of a common brain template using FreeSurfer. The AMT is then normalized in each subject so that the lowest AMT over all coil locations is 1. For each point on the template brain, the electric field data of all coil locations are normalized so that the electric field for the central coil location is 1. This normalization removes the subject-specific terms A_j and B_j in (1), and the relationship between the AMT and inverse of the electric field can be investigated using simple linear regression. The linear regression analysis is repeated for each point on the template brain surface. This process produces a whole-brain map of the Pearson correlation coefficient that indicates the cortical areas where there is an agreement between the AMT and the inverse of the electric field normal component or magnitude. Figure 5 (A) illustrates the Pearson correlation coefficient over the left hemisphere calculated for the magnitude ($|E|$) and normal component (E_n) of the electric field. The global maximal correlation (0.81) was found for $|E|$ and was

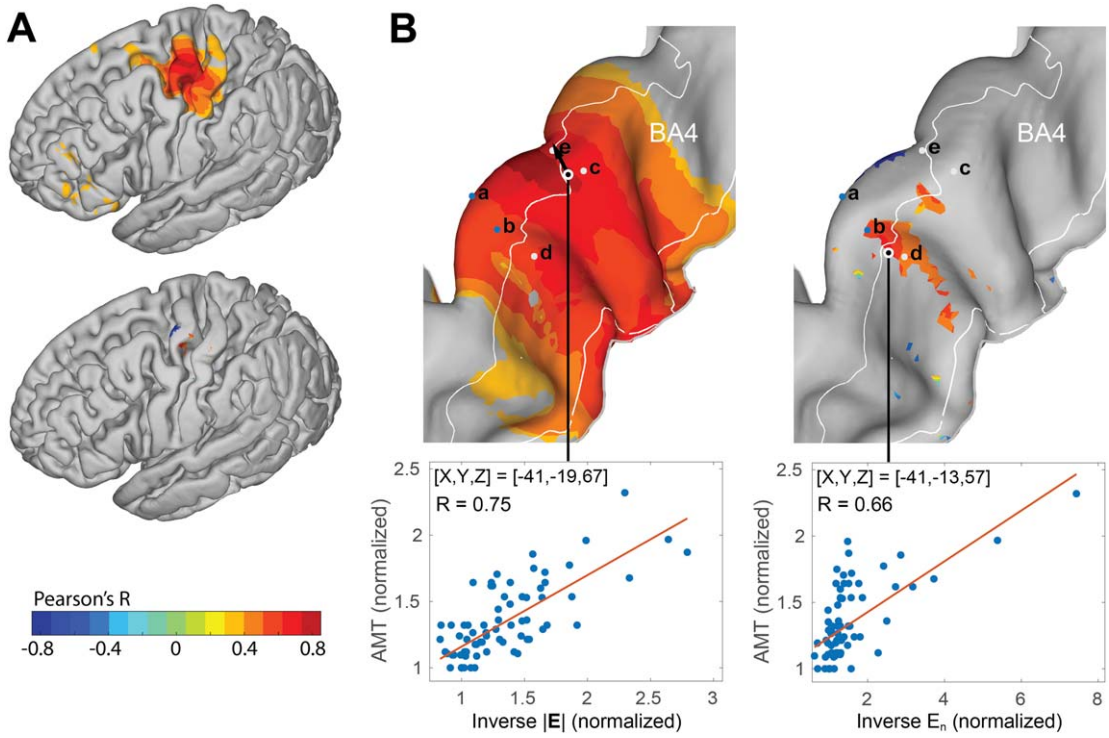

Figure 5. (A) Pearson correlation coefficient between the normalized AMTs and the inverse of the normalized electric fields on template brain for the magnitude (upper) and the normal component (lower). (B) Close-up view of the posterior wall of the central sulcus on template brain shows the points with the strongest correlation (white circle with a black centre). The strongest correlation points for the magnitude (a) and the normal component (b) from Laakso *et al* (2018) are marked as blue dots. The light grey dots indicate the cortical FDI target locations obtained from the studies of Bungert *et al* (2017) (c), Kataja *et al* (2021) (d), and Numssen *et al* (2021) (e). Grey areas indicate locations where the correlation is not significant at false discovery rate of 0.05. The data for Figure 5 are provided at https://doi.org/10.17605/OSF.IO/6J2RB.

located in $[-31, -12, 60]$ in MNI coordinates. This location corresponded to the anterior wall of the precentral gyrus (Brodmann area 6). However, high correlations were also found on the crown and the posterior wall of the precentral gyrus. As the motor responses produced by TMS are thought to follow from the activation of the primary motor cortex, we will only focus on Brodmann area 4 in the following.

The maximal Pearson correlation coefficients in Brodmann area 4 were 0.75 and 0.66 for $|E|$ and E_n, respectively. The locations of these maximal correlations in MNI coordinates were $r_{|E|} = [-41, -19, 67]$ and $r_{E_n} = [-41, -13, 57]$, respectively (figure 5).

Similarly to the preregistered target location, the linear mixed effect model was used to investigate the relationship between the AMT and $|E|$ at the $r_{|E|}$. One outlier was left out from the model fit. The estimates for the parameters are listed in table 2. The relationship between the AMT and $|E|$ obtained from the model is illustrated in figure 4(B). The intercept still differed from zero but not as much as in the preregistered model fit. The effect of the electric field was also stronger and closer to the inverse relationship.

3.4. Exploratory: removing bias in the predicted optimal coil location using an improved cortical target location

We moved the cortical target location of the FDI muscle to the two locations obtained from the correlation study above, and repeated the coil location optimization procedure (section 2.5) using the new target locations. For the optimization using $r_{|E|}$ as the cortical target location, the maximized electric field component was in the direction of $[0.62, 0.62, 0.48]$ in the MNI coordinates instead of the normal component. This electric field component direction was the one that produced the largest correlation between the AMT and the normalized inverse of the electric field at $r_{|E|}$.

The results are listed in table 3. The coil location optimized using $r_{|E|}$ as the cortical target did not show bias in the LM nor PA direction compared to the measured hotspot location. Using the r_{E_n} as the cortical target showed bias in PA direction. Chi-square test did not support the SD being smaller than 1 cm for $r_{|E|}$ (LM: $\chi^2(8, N = 9) = 7.17, p = 0.48$, PA: $\chi^2(8, N = 9) = 6.10, p = 0.36$) nor r_{E_n} (LM: $\chi^2(8, N = 9) = 4.52, p = 0.19$, PA: $\chi^2(8, N = 9) = 6.79, p = 0.44$).

Table 3. Summary statistics of the distances between the measured hotspot and the predicted optimal coil location. The prediction was obtained for the preregistered cortical target locations and for exploratory targets $r_{|E|}$ and r_{E_n}.

Target	Distance	Mean (cm)	SD (cm)	Range (cm)
Preregistered	Euclidean	1.30	0.54	0.37–2.09
target	LM	-0.06 ($t(8) = -0.27, p = 0.79$)	0.67	-0.85 to 1.06
$[-41, -7, 63]$	PA	0.83 ($t(8) = 3.22, p = 0.01$)	0.77	-0.33 to 1.74
$r_{\|E\|}$	Euclidean	1.35	0.55	0.54–2.27
$[-41, -19, 67]$	LM	0.39 ($t(8) = 1.24, p = 0.25$)	0.95	-1.18 to 1.55
	PA	0.25 ($t(8) = 0.84, p = 0.42$)	0.87	-1.14 to 1.52
r_{E_n}	Euclidean	1.41	0.69	0.16–2.43
$[-41, -13, 57]$	LM	-0.23 ($t(8) = -0.92, p = 0.38$)	0.75	-1.20 to 1.02
	PA	0.82 ($t(8) = 2.67, p = 0.03$)	0.92	-0.51 to 2.18

4. Discussion

In this study, we investigated whether we can reliably predict the optimal coil positioning and estimate the MT values using induced electric fields calculated with computational dosimetry. The mean Euclidean distance between the predicted optimal coil locations and measured hotspots was 1.3 cm, and the mean distances in lateral-medial and posterior-anterior directions were 0.06 cm and 0.83 cm, respectively.

Unlike hypothesized, the hotspot prediction was not able to attain the 1 cm accuracy. Nevertheless, the predictions were still in close proximity of the measured hotspots (1.3 ± 0.54 cm), and compared to the state of the art in TMS hotspot search, the difference in the accuracy was small. Previous studies have evaluated the reliability of the manual hotspot search of different muscles by comparing the measured hotspot locations between sessions in individual subjects. The distance between the hotspots varies slightly between different studies, but seems to consistently be approximately 1 cm (Wolf *et al* 2004, Forster *et al* 2012, Sollmann *et al* 2013, Weiss *et al* 2013, Cotovio *et al* 2021). Especially relevant is the study using the FDI muscle in which the distances were 1.16 ± 0.62 cm (Forster *et al* 2012). The result is comparable to our result. Thus, we believe that our method, even in its current state, could improve the speed and reliability of the TMS hotspot finding procedure.

The inverse of $E_{n,\mathrm{FDI}}$ had a significant effect on the AMT but was not alone enough to predict the AMT. Based on data from Laakso *et al* (2018), we expected an inverse relationship between the electric field normal component and the AMT at the cortical location determined in the study ($[-41, -7, 63]$ in MNI coordinates), but the relationship we found differed from the expected ideal inverse proportionality.

There are several potential reasons why the $E_{n,\mathrm{FDI}}$ was not inversely proportional to the AMT. One potential reason is that the preregistered target from the study of Laakso *et al* (2018) might not be generalizable to the subjects of this study. In addition, there may be uncertainty in the location because Laakso *et al* (2018) did not use a neuronavigation system. Another reason is that the targeted electric field component (normal) may be suboptimal. For example, Bungert *et al* (2017) found that the magnitude correlated better with the MT than the normal component. Additionally, other studies have found different locations for the FDI muscle, such as $[-37, -19, 66]$ (Bungert *et al* 2017), $[-34, -14, 67]$ (Numssen *et al* 2021), or $[-42, -15, 57]$ (the mean from Kataja *et al* (2021)), so there is no clear consensus of the exact location.

Considering the results, we relocalized the cortical targets with the data from this study using the method of Laakso *et al* (2018). The data indicated a more posterior cortical target location ($[-41, -19, 67]$) compared to the preregistered target (Laakso *et al* 2018), and this new target location also agrees with the locations found in the studies of Bungert *et al* (2017) and Numssen *et al* (2021). Additionally, our results showed that the predicted optimal coil locations were systematically too anterior compared to the measured hotspot, which could also be explained by a too anterior preregistered target location. Another possible reason for a systematic error is the difference between a supine position in MRI and a sitting position in TMS, which slightly shifts the location of the brain inside the skull (Mikkonen and Laakso 2019). However, our predicted locations were too anterior, whereas the change in position should cause the predicted locations to be too posterior as the brain shifts to anterior, so the brain shift is not a probable explanation for our result. Therefore, better selection of the target location could improve the accuracy of the coil location optimization procedure. We tested this by trying two cortical target locations as discussed. Using the location $r_{|E|}$ which had the strongest correlation with the $|E|$ in Brodmann area 4 removed the bias but did not reduce the distance.

Although the coil location optimization method is already potentially useful, the study has some limitations. One limitation of the current study is that this method fails to properly consider the individual functional differences. As the cortical target location is derived from a group analysis on a template brain, it does not

completely consider the individual variations of the cortical target location, which is demonstrated in Kataja *et al* (2021). These inter-individual differences can potentially explain the observed variations in the distances between the predicted and the measured hotspots. Another limitation is the selection of the cortical target location, which is essential for the method. So far, only few cortical targets have existing coordinate data, which reduces the potential applications for the method. Additionally, the selection of a single target location is a simplification, as TMS could activate multiple cortical locations that cause a motor response. This could explain why the relationship between the electric field and the AMT was not ideally inversely proportional.

In conclusion, we showed that dosimetric modelling can be used to predict the hotspot coil location when the cortical target location in a template brain is known. The accuracy of the predicted optimal coil locations is comparable to manual hotspot search. Dosimetric models could provide individually optimized coil location and direction using only MR images, without stimulating the patient even once. Our study demonstrated the feasibility of the method on the motor cortex, as finding the target locations there is fairly straightforward by measuring MEPs from the specific muscle. Theoretically, the method could be used for locating any part of the cerebral cortex. However, more research is required for the selection of the correct cortical target locations.

Acknowledgments

This work was supported by the Academy of Finland [Grant No. 325326].

Data availability statement

The data cannot be made publicly available upon publication due to legal restrictions preventing unrestricted public distribution. The data that support the findings of this study are available upon reasonable request from the authors.

Conflict of interest

The authors declare no financial or non-financial competing interests.

Preregistration

This study was preregistered on the open science framework (https://doi.org/10.17605/OSF.IO/MA2JT). The following changes are made to the preregistration:

(1) Description of change: Limited the MSO intensity to 61% prior to the measurements.
Rationale: Limitation reduces the time required for the measurements.
Effect of change on study results: None expected.

(2) Description of change: Changed the grid size from 5 to 4 cm for the TMS prior to the measurements.
Rationale: Coil locations too far away from the motor cortex might not provide MEPs.
Effect of change on study results: None expected.

ORCID iDs

Noora Matilainen https://orcid.org/0000-0002-9079-2093
Juhani Kataja https://orcid.org/0000-0002-1212-0080
Ilkka Laakso https://orcid.org/0000-0002-8162-1356

References

Aberra A S, Wang B, Grill W M and Peterchev A V 2020 Simulation of transcranial magnetic stimulation in head model with morphologically-realistic cortical neurons *Brain Stimul.* **13** 175–89

Aonuma S, Gomez-Tames J, Laakso I, Hirata A, Takakura T, Tamura M and Muragaki Y 2018 A high-resolution computational localization method for transcranial magnetic stimulation mapping *Neuroimage* **172** 85–93

Baeken C *et al* 2019 Repetitive transcranial magnetic stimulation treatment for depressive disorders: current knowledge and future directions *Curr. Opin. Psychiatry* **32** 409–15

Bungert A, Antunes A, Espenhahn S and Thielscher A 2017 Where does tms stimulate the motor cortex? combining electrophysiological measurements and realistic field estimates to reveal the affected cortex position *Cerebral Cortex* **27** 5083–94
Cotovio G, Oliveira-Maia A J, Paul C, Viana F F, da Silva D R, Seybert C, Stern A P, Pascual-Leone A and Press D Z 2021 Day-to-day variability in motor threshold during rtms treatment for depression: clinical implications *Brain Stimul.* **14** 1118–25
Dale A M, Fischl B and Sereno M I 1999 Cortical surface-based analysis: I. segmentation and surface reconstruction *NeuroImage* **9** 179–94
Fischl B, Sereno M I and Dale A M 1999 Cortical surface-based analysis: II: inflation, flattening, and a surface-based coordinate system *NeuroImage* **9** 195–207
Fonov V *et al* 2011 Unbiased average age-appropriate atlases for pediatric studies *NeuroImage* **54** 313–27
Fonov V S, Evans A C, McKinstry R C, Almli C and Collins D 2009 Unbiased nonlinear average age-appropriate brain templates from birth to adulthood *NeuroImage* **54** 313–27
Forster M-T, Senft C, Hattingen E, Lorei M, Seifert V and Szelényi A 2012 Motor cortex evaluation by ntms after surgery of central region tumors: a feasibility study *Acta Neurochirurgica* **154** 1351–9
Gomez-Tames J, Laakso I and Hirata A 2020 Review on biophysical modelling and simulation studies for transcranial magnetic stimulation *Phys. Med. Biol.* **65** 24TR03
Hallett M 2000 Transcranial magnetic stimulation and the human brain *Nature* **406** 147–50
Kataja J, Soldati M, Matilainen N and Laakso I 2021 A probabilistic transcranial magnetic stimulation localization method *J. Neural Eng.* **18** 0460f3
Laakso I, Murakami T, Hirata A and Ugawa Y 2018 Where and what TMS activates: experiments and modeling *Brain Stimul.* **11** 166–74
Laakso I, Tanaka S, Koyama S, De Santis V and Hirata A 2015 Inter-subject variability in electric fields of motor cortical tdcs *Brain Stimul.* **8** 906–13
Matilainen N, Soldati M and Laakso I 2022 The effect of inter-pulse interval on tms motor evoked potentials in active muscles *Front. Human Neurosci.* **16**
Meincke J, Hewitt M, Batsikadze G and Liebetanz D 2016 Automated tms hotspot-hunting using a closed loop threshold-based algorithm *NeuroImage* **124** 509–17
Mikkonen M and Laakso I 2019 Effects of posture on electric fields of non-invasive brain stimulation *Phys. Med. Biol.* **64** 065019
Numssen O, Zier A-L, Thielscher A, Hartwigsen G, Knösche T R and Weise K 2021 Efficient high-resolution tms mapping of the human motor cortex by nonlinear regression *NeuroImage* **245** 118654
Rossini P M *et al* 2015 Non-invasive electrical and magnetic stimulation of the brain, spinal cord, roots and peripheral nerves: basic principles and procedures for routine clinical and research application. an updated report from an ifcn committee *Clin. Neurophysiol.* **126** 1071–107
Saturnino G B, Thielscher A, Madsen K H, Knösche T R and Weise K 2019 A principled approach to conductivity uncertainty analysis in electric field calculations *NeuroImage* **188** 821–34
Siebner H R *et al* 2022 Transcranial magnetic stimulation of the brain: What is stimulated?-a consensus and critical position paper *Clin. Neurophysiol.* **140** 59–97
Sollmann N, Hauck T, Obermüller T, Hapfelmeier A, Meyer B, Ringel F and Krieg S M 2013 Inter-and intraobserver variability in motor mapping of the hotspot for the abductor policis brevis muscle *BMC Neurosci.* **14** 1–7
Stilling J M, Monchi O, Amoozegar F and Debert C T 2019 Transcranial magnetic and direct current stimulation (TMS/tDCS) for the treatment of headache: a systematic review *Headache: J. Head Face Pain* **59** 339–57
Tervo A E, Metsomaa J, Nieminen J O, Sarvas J and Ilmoniemi R J 2020 Automated search of stimulation targets with closed-loop transcranial magnetic stimulation *Neuroimage* **220** 117082
Thielscher A, Opitz A and Windhoff M 2011 Impact of the gyral geometry on the electric field induced by transcranial magnetic stimulation *Neuroimage* **54** 234–43
Weise K, Numssen O, Thielscher A, Hartwigsen G and Knösche T R 2020 A novel approach to localize cortical tms effects *Neuroimage* **209** 116486
Weiss C, Nettekoven C, Rehme A K, Neuschmelting V, Eisenbeis A, Goldbrunner R and Grefkes C 2013 Mapping the hand, foot and face representations in the primary motor cortexretest reliability of neuronavigated tms versus functional mri *Neuroimage* **66** 531–42
Wolf S L, Butler A J, Campana G I, Parris T A, Struys D M, Weinstein S R and Weiss P 2004 Intra-subject reliability of parameters contributing to maps generated by transcranial magnetic stimulation in able-bodied adults *Clin. Neurophysiol.* **115** 1740–7